Development of Differential Amplifier Circuits Based on Radiation Diamond hardened H-diamond MOSFET (RADDFET)

Hiroki. Fukushima[1], Manobu. M. Tanaka[2], Hitoshi. Umezawa[3], Hiroyuki. Kawashima[3], Tadashi. Masumura[1], Masaya. Miyahara[2], Yusei. Deguchi[1.3], Naohisa. Hoshikawa[1] and Junichi.H. Kaneko[1]
[1] *Graduate School of Engineering, Hokkaido University, Kita 13 Nishi, 8, Kita-ku, Sapporo,060-8628, Japan*
[2]*IPNS, KEK, Oho1-1, Tsukuba, Ibaraki, 298-864-5405, Japan*
[3] *AIST,1-8-31 Midorigaoka, Ikeda, Osaka 563-8577, Japan*
hito-1zerosa15ki@eis.hokudai.ac.jp

Abstract

As one part of the development of electronic devices for use in high-temperature and high-radiation environments, especially for use in containment vessels of nuclear power plants, a differential amplifier circuit based on hydrogen-terminated diamond MOSFETs that have excellent radiation resistance and high-temperature operational capability were designed and fabricated. The 14 diamond MOSFETs were made using the same design on a 4-mm-square diamond single-crystal substrate. A FET model was fabricated from measured FET characteristics. Then the performance of differential amplifier circuit was simulated using the LTspice code. A differential amplifier part was formed using a pair of diamond MOSFETs with similar characteristics. In all, six diamond MOSFETs were used to construct the differential amplifier circuit. Then the circuit was operated in both inverting and non-inverting output modes. The maximum amplification factor was 4.7 for the non-inverting output at room temperature.

Keyword: Diamond , MOSFET, Differential amplification, radiation resistance

1. Introduction

The core meltdown accident at the Fukushima Daiichi Nuclear Power Plant in March 2011, the upper operating temperature and allowable radiation dose requirements for equipment used inside of reactor containment vessels in Japan were raised. As some requirements, the containment atmosphere monitoring system (CAMS) must accommodate an operating temperature of 300°C (72 hr) and an integrated dose of 5 MGy [1]. In addition, although high-temperature operation is not necessary, electronic devices with radiation resistance to doses of a few MGy are necessary for use with the Fukushima Daiichi Nuclear Power Plant decommissioning project. In addition to nuclear power plants, needs exist for electronic devices with excellent radiation resistance in high-energy accelerators, medical irradiation equipment, space, and other fields.

For high-energy physics experiments using high-energy accelerators, electronic circuits that perform complex processing for large-scale detection devices are fabricated using Si integrated circuit technology. Devices with radiation resistance to doses of a few MGy are in practical use [2]. However, the use of Si in high-temperature operating environments is hopeless. Even when SOI technology is used, the upper limit is around 200°C, rendering long-term stable operation difficult.

To overcome this difficulty, research and development have been conducted using wide bandgap semiconductors such as SiC [3–5] and GaN [6]. For example, a transistor impedance amplifier (TIA) consisting of CMOS transistors in SiC has been reported to functions with a total dose of up to 1 MGy [7],[8].

Diamond has a forbidden bandwidth of 5.47 eV, which is wider than that of either SiC and GaN [9]. It also has low γ-ray sensitivity because of its atomic number (6), high breakdown electric field of 10 MV/cm, and high thermal conductivity of 20 W/cm-K [10]. These characteristics indicate diamond as a promising material for radiation-resistant and high-temperature-operation semiconductor devices. In the early 1990s, high-temperature operation of diamond field-effect transistors (FETs) doped with boron as an acceptor was reported [11]. At that time, diamond FETs had low drain current. Their low device performance such as drain current density, transconductance, and threshold voltage were affected strongly by temperature.

Because diamond Metal Semiconductor Field Effect Transistors (MESFETs) can simplify the device structure, fabrication process, and can be miniaturized compared with other FET types: high-frequency diamond MESFETs that had 45 GHz transition frequency [12]; and 2.1 W /mm output power density (at 1 GHz) [13] have been reported by adoption of hydrogen-terminated diamond surfaces. Furthermore, from the viewpoint of radiation resistance, diamond MESFETs have been developed because they have no insulating layer that leads to charge accumulation caused by radiation. Moreover, reports have described tolerance against integrated doses of 10 MGy or higher and an operating temperature of 450°C [14]. Nevertheless, low drain current and low mutual conductance of diamond MESFETs persist as shortcomings. Moreover, the high noise level presents difficulties of developing a preamplifier based on the diamond MESFET [15].

Metal-Oxide-Semiconductor Field Effect Transistor (MOSFET) [16]–[18] is another typical structure of field-effect transistors. In the case of diamond, hydrogen-terminated surface conduction layers are often used. This type of diamond MOSFET represents marked improvements of drain current and mutual conductance compared with these characteristics of typical diamond MESFETs [19],[20]. With power semiconductor applications in mind, Kawarada et al. reported a diamond MOSFET that operates at 400°C by adoption of an Al_2O_3 gate dielectric and passivation layer on the hydrogen-terminated diamond surface [21].

From the viewpoint of radiation resistance, although the gate dielectric and passivation layer are expected to protect the hydrogen-terminated surface conduction layer that is indispensable to achieve high mutual conductance, some risk exists of charge accumulation by irradiation. Yamaguchi et al. attempted to develop a hydrogen-terminated surface conduction layer diamond MOSFET, known as a Radiation Diamond hardened H-diamond MOSFET (RADDFET), and eventually achieved mutual conductance of 3.0 mS/mm and radiation resistance of 1 MGy [22]. In fact, RADDFETs have been demonstrated to have radiation resistance of 3 MGy and beyond [23].

This article describes a differential amplification circuit that is necessary for a front-end amplifier based on the RADDFET. For this purpose, to obtain a pair of RADDFET with similar characteristics, 8–14 RADDFETs of identical design were fabricated on diamond single-crystal substrates. Moreover, based on the measured FET characteristics of these RADDFETs, a differential amplification circuit was designed using LTspice code. Then the real circuit was fabricated and evaluated.

2. **Experimental**

2.1. Fabrication of RADDFETs

Although RADDFETs have excellent properties of high-temperature operation and radiation resistance, obtaining RADDFETs that have the same characteristics as those of other substrates is difficult because the sheet resistance and density of defects differ among diamond substrates. Obtaining a pair of RADDFETs that have similar characteristics is indispensable for making a differential amplification circuit, 8–14 RADDFETs having the same design were fabricated on one diamond substrate.

Figure 1 shows a schematic drawing of the RADDFET fabrication process. First, 1 μm of undoped diamond layers were grown homoepitaxially on a single diamond substrate making use of MWCVD. Then a SiO_2 film was synthesized over the entire surface of the device after strong acid cleaning by microwave-assisted plasma CVD, a mask was formed by dry etching only for the source-drain region, and a 0.2 µm of p+ layer was grown selectively by thermal filament (HF)CVD [24],[25]. Then, after the diamond surface was selectively hydrogen-terminated using a microwave-assisted plasma CVD system [26] and oxygen-terminated , 40 nm of Al_2O_3 layer was deposited at 450°C using an atomic layer deposition system (FlexAL;

Oxford Instruments Plc.). The Ru/Au multilayer electrodes were then formed by RF sputtering.

As shown in Figure 2 a), 14 FETs were fabricated on a 4-mm-square diamond single-crystal substrate. Each RADDFET was mounted in a package, bonded, and used in an actual circuit, as shown in Figure 2 c). The typical performance values of the fabricated FETs were 2 mS/mm g_m, with 25 mA/mm drain current. Six of these FETs were used in a differential amplifier circuit.

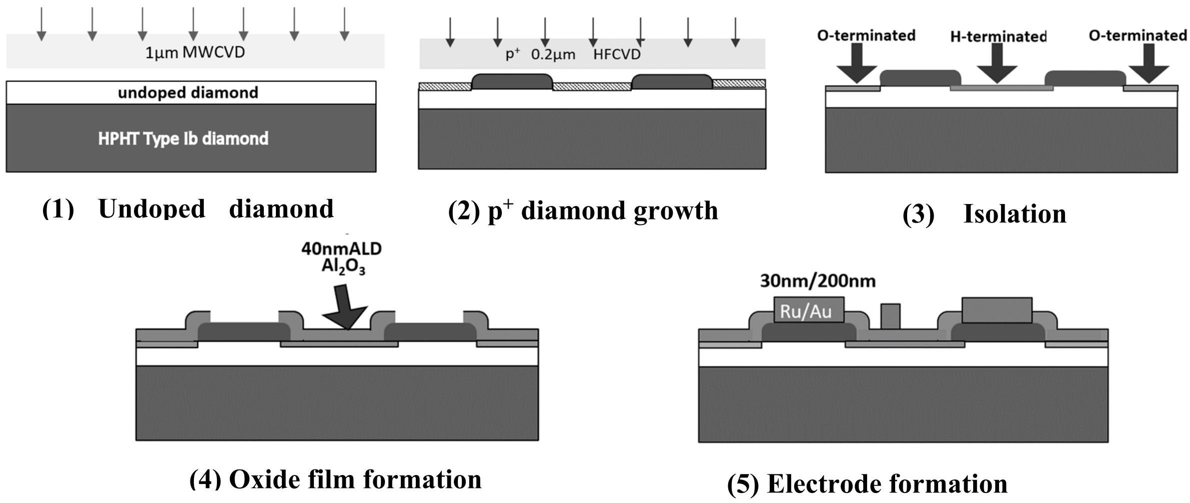

Figure 1: FET fabrication process: (1) homoepitaxial growth of undoped diamond layer on a single crystal diamond substrate; (2) p+ layer growth by HFCVD method; (3) hydrogen termination (conductive layer) and oxygen termination (device separation) by the CVD system; (4) fabrication of Al_2O_3 layer grown using an atomic layer deposition system, and (5) Ru/Au electrode formation using RF sputter.

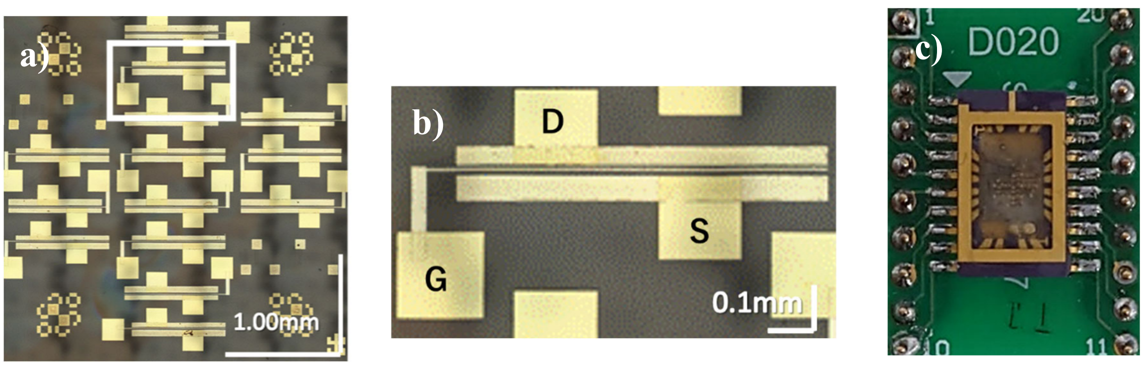

Figure 2: Fabricated RADDFETs: a) 14 RADDFETs on a 4-mm-square diamond single-crystal substrate, b) magnified view of one RADDFET element, and c) packaged RADDFETs.

2.2. Circuit simulation

Although the FETs were fabricated using the same design on the same substrate (The standard deviation of the FET threshold used was 1.35), it was expected that operating characteristics such as the threshold voltage would differ for each FET because of the bias of fixed charge in the alumina passivation layer, and other factors. To address this issue of difference, the differential amplification part was designed as shown in Figure 3 to adjust the bias voltage separately for each FET.

For differential amplifier circuit fabrication, two FETs (FET-A and FET-B, Figure 4) that had similar threshold voltages and I_d-V_d characteristics were used as the differential pair (Threshold voltage: FET-A=-5.6 V, FET-B=-3.3 V). One other FET on the same substrate (FET-C, Figure 4) was used for current regulation. Another three were used for noise reduction.

To predict the applied voltage at which the differential amplifier circuit functions, device simulation was conducted using the LTspice code. For this purpose, an FET model was created based on the measured I_d-V_d characteristics of the fabricated RADDFETs. Table 1 shows a representative list of designed FETs. Examples of I_d-V_d characteristics of the RADDFETs and the FET models used for simulation are shown in Figure 4. There is a significant difference in the behavior between the simulated and real devices from the time the threshold voltage is exceeded until the saturation region is reached. The increase in drain current after the threshold is steeper in the real device, and the simulation reaches the saturation region more quickly. This is expected to be due to the accuracy of the transfer conductance. As Figure 3 shows, applied voltages for the parts were fixed by the simulation respectively as follows: V^+, 36 V; V^-, -36 V; V_{ref}, 1.66 V; and V_b, 10.5 V. For this condition, an amplification factor of approximately 4.4 times was obtained. At this time, the V_g of FET-C is V_g=13.5 V, and the drain current is around 6 mA. Figure 5 presents examples of input and output signals of the differential amplification circuit settled at each bias voltage described above, as calculated using LTspice code.

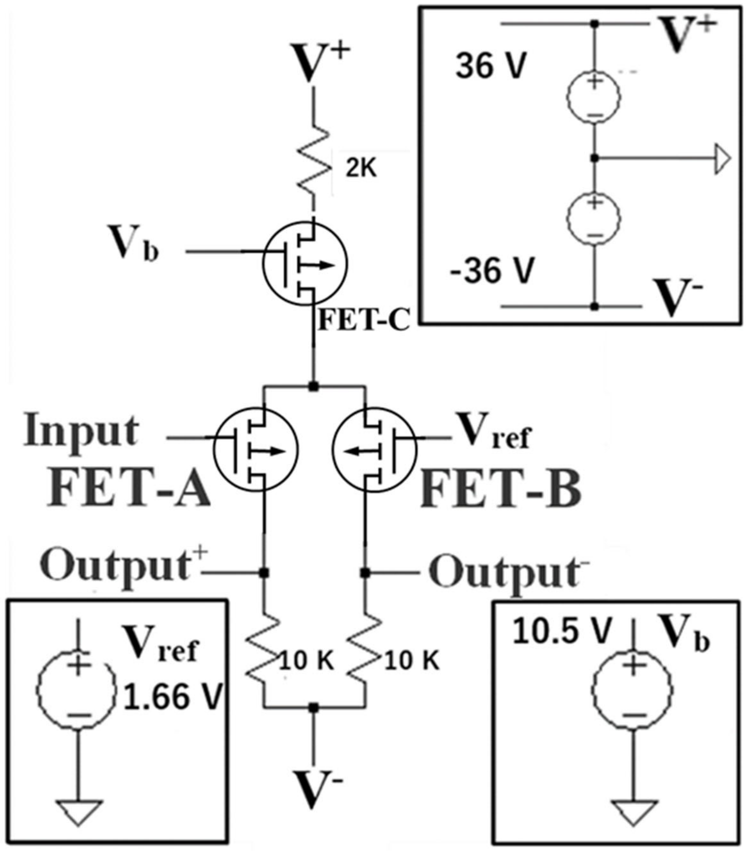

Figure3: Part of the differential pair portion of the designed differential amplifier circuit (FET-A, B shown in Figure 4 are designed as differential pairs).

Table1 : Parameters of the created FET model (partial)

	FET-A	FET-B	FET-C
threshold voltage Vto (V)	-5.6	-3.3	-5
transfer conductance Kp (A/V^2)	0.30m	0.165m	0.165m
channel modulation factor λ (1/V)	1.42m	0.18m	8.9m

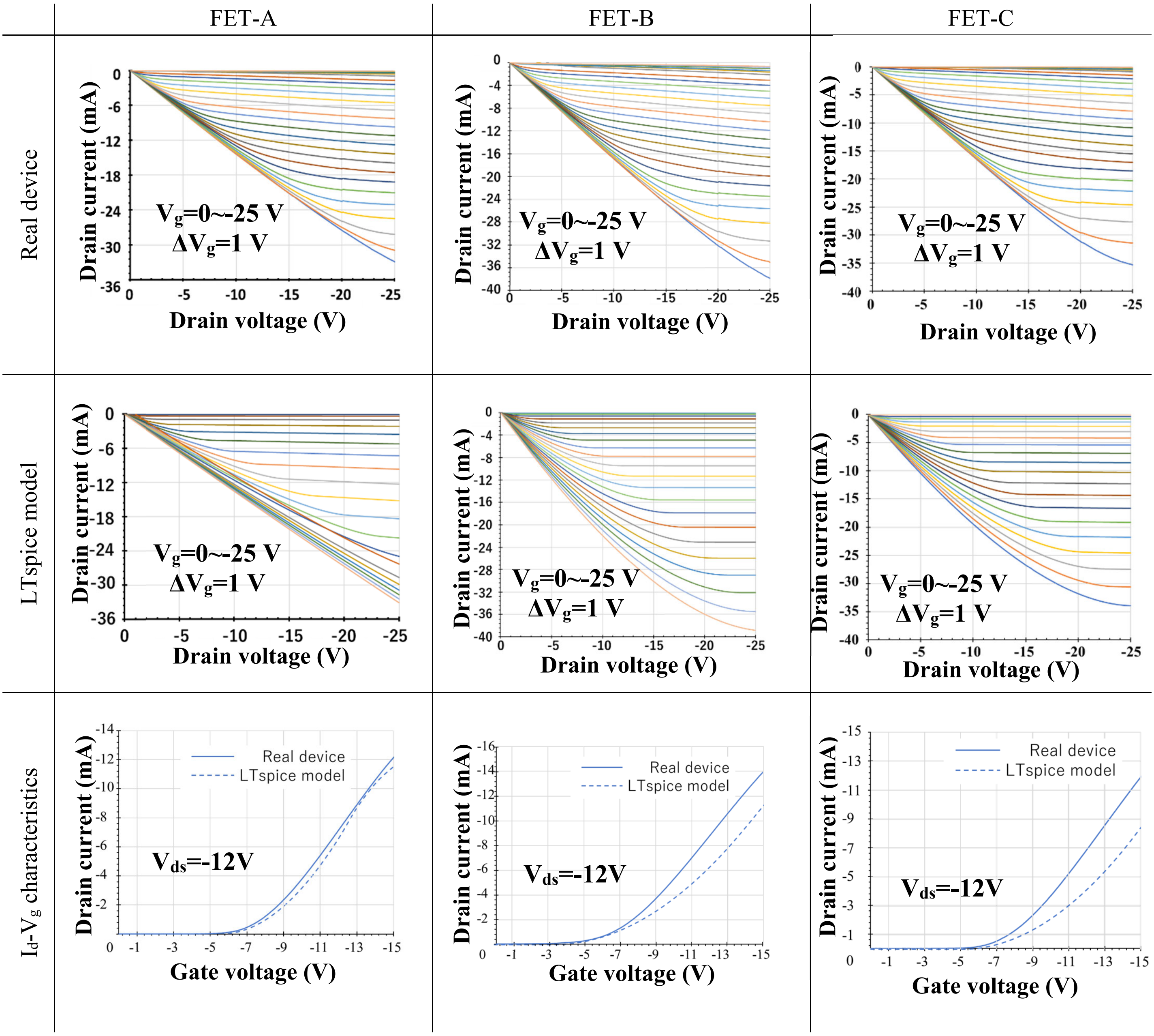

Figure 4: I_d-V_d curves and I_d-V_g characteristics of FET elements used in differential pairs:
in I_d-V_d curves, gate voltage measured in the range of 0 to -25 V; drain voltage measured in the range of 0 to -25 V;
above, real element; below, LTspice model fabricated from the readout characteristics.
In Id-Vg characteristics, gate voltage measured in the range of 0 to -15 V; drain voltage measured in -12 V.

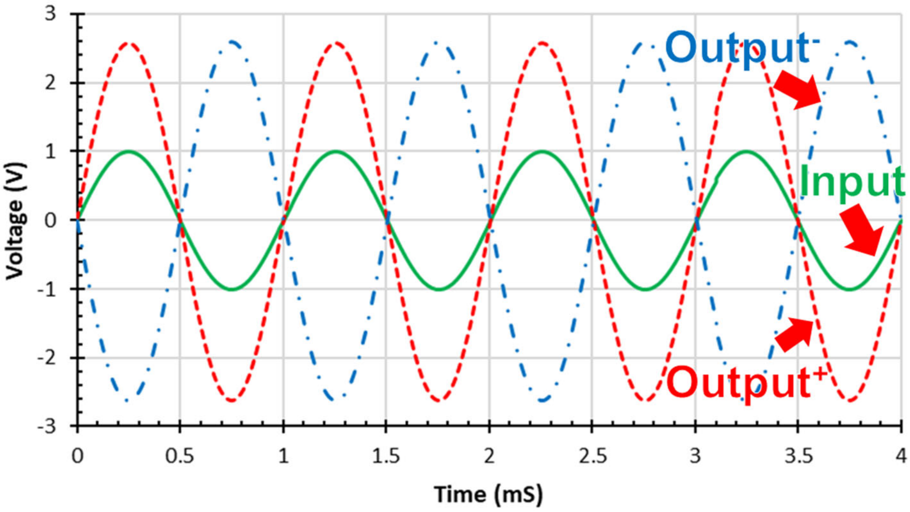

Figure 5: Examples of input–output characteristics obtained from the LTspice simulation: V^{+}, 36 V; V^{-}, -36 V; V_{ref}, 1.66 V; V_{b}, 10.5 V; V^{+}, V^{-}, V_{ref}, V_{b} see Figure 3 offset voltage 4.34 V output^{+}, 4.67 V output.

2.3. Circuit implementation

The circuit designed based on the simulations was implemented as shown in Figure 6. As described above, two RADDFETs were used for a differential amplification pair. One RADDFET was used for current regulation. The other three were used for noise reduction. This time evaluation was conducted only at room temperature. Therefore, an ordinary PCB circuit board, resistors, capacitors, and solder were used.

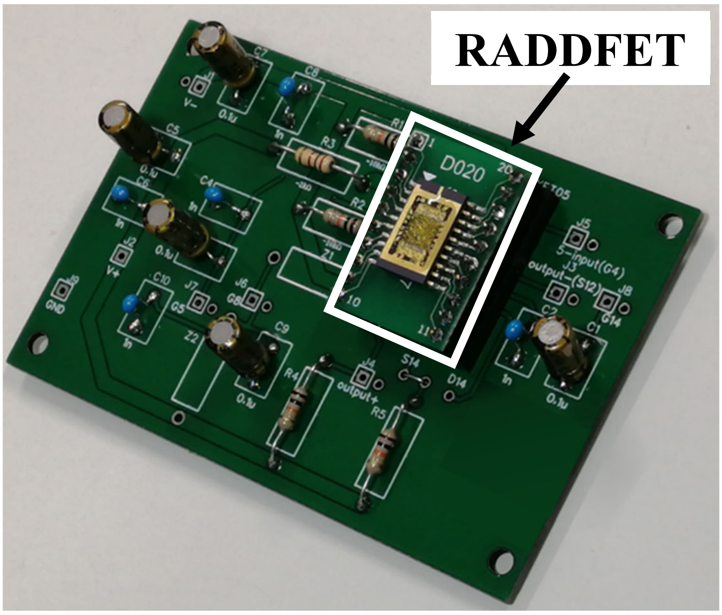

Figure 6: Fabricated differential amplifier circuit (RADDFETs and non-RADDFET elements are enclosed by in the white box. The substrate is an existing product because it is assumed to operate at room temperature).

3. Experiment Results and Discussion

As applied voltages, as shown in Figure 3, we set the following: V^{+}, 36 V; V^{-}, -36 V; V_{ref}, 1.66 V; and V_{b}, 10.5 V. Then signal amplification began. The input signal was a sine wave of 1 V. As Figure 7 a) shows, only non-inverting amplification was observed without inverting amplification. The amplification factor was approximately 4.7 times. Some differences were found between results obtained using the simulation. They were attributable to a difference in threshold voltages between the real RADDFETs and the FET model.

The bias voltage was changed subsequently as follows: V^{+}, 43 V; V^{-}, -30 V; V_{ref}, 3 V; and V_{b}, 10 V. Here, the V_g of FET-C was V_g=13.3 V and the drive current was 6 mA. Inverting and non-inverting outputs were obtained simultaneously, as shown in Figure 7 b). Amplitudes were 0.3 and 1.6 times, respectively, for inverting and non-inverting outputs. Then, the device was broken due to overvoltage, during evaluating of the bias dependence.

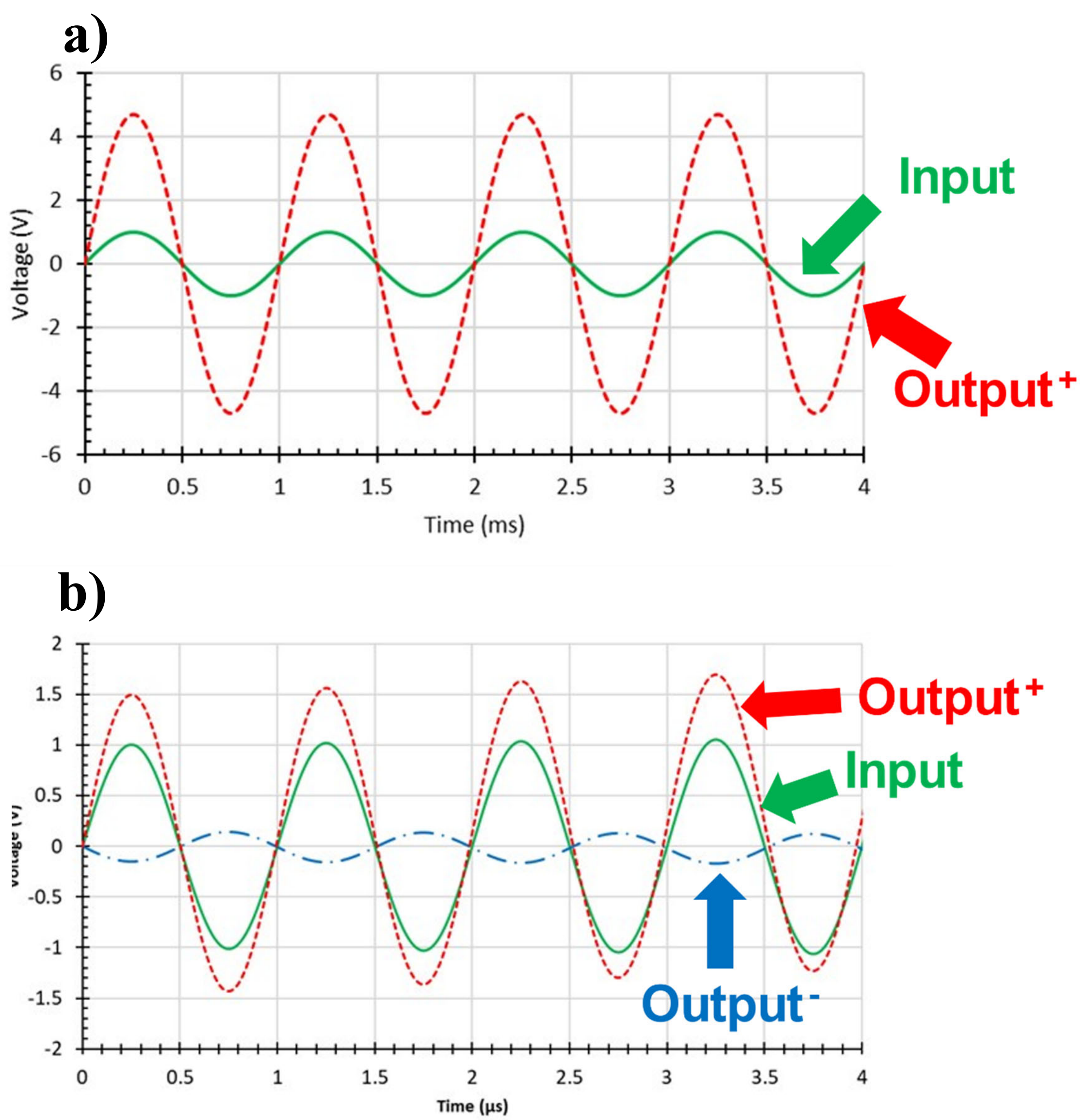

Figure 7: Circuit input–output according to the set voltage values shown in Figure 3: a) offset voltage 16 V output$^+$, omitted output$^-$ (4.7 times multiplication factor); b) offset voltage 2.5 V output$^+$, -0.63 V output$^-$ (0.3 times inverting, 1.6 times non-inverting multiplication factors).

The differences in output characteristics between the simulation example shown in Figure 5 and the actual circuit shown in Figure 7 are attributable to the FET model accuracy. To fabricate a complex circuit such as a diamond operational amplifier or diamond ICs, brush up fabrication techniques must be used to obtain design characteristics, e.g., I_d-V_d characteristics and threshold voltage.

To obtain diamond FETs that have the same threshold voltage, reducing the footprint of each FET and concentrating them in a small area is effective because it suppresses variation of the sheet resistance of the hydrogen-terminated diamond surface, doping density, and charge distribution in the gate dielectric film that occur even in the same substrate and technology.

In addition, the mutual conductance of FET devices fabricated on the same substrate is distributed according to a Gaussian distribution [27]. The following relation holds between mutual conductance and the threshold voltage.

$$g_m = \beta\left(V_{gs} - V_{th}\right) \qquad \left(\beta = \frac{w_g \mu C_{ox}}{L_g}\right)$$

Therein, g_m represents the transconductance, V_{gs} signifies the gate-source voltage, V_{th} expresses the threshold voltage, w_g denotes the channel width, L_g stands for the channel length, μ is the electron mobility, and C_{OX} denotes the capacitance per unit area of the insulating film.

As mentioned above, the mutual conductance consists of V_{gs} and V_{th}. Considering that V_{gs} is constant, variation of the threshold voltage also follows the variation of a Gaussian distribution. Therefore, if the number of FETs is increased, convergence of the threshold voltage can be expected from the central maximum theorem. For this study, 14 FETs were fabricated on a single-crystal substrate. If 56 FETs are fabricated in the same area, then the standard error will be 1/2 from the central limit theorem. Naturally, in this case, the parameters of the FETs converge, the number of FETs with uniform characteristics increases, and the number of FETs that can be extracted is also increase. Therefore, fabricating FETs with similar characteristics on the same substrate with a smaller footprint is effective. This method is expected to be crucially important for realizing diamond ICs.

4. Conclusion

For this study, a prototype differential amplifier circuit was fabricated based on hydrogen-terminated diamond MOSFETs (RADDFETs) that have excellent radiation resistance and high-temperature operation capability. Inverting and non-inverting amplification operations were performed. An amplification factor of up to 4.7 times was obtained at the non-inverting output. The difference in input–output characteristics between the simulation and the actual circuit was attributable to the difference between the model and the actual device. For future development of diamond ICs, making the device characteristics uniform is expected to be necessary. As a countermeasure, we expect to promote improvements centered on reduction of the area of the device footprint and improvement of the uniformity of FET characteristics such as threshold voltage.

Furthermore, capacitors, resistors, packages, circuit boards, and other components for high-temperature operation must be developed. These developments have been achieved in parallel with the aim of progression to the development of electronic devices that have high radiation resistance and capabilities for high-temperature operation.

Acknowledgement

Part of this research was supported by MEXT Innovative Nuclear Research and Development Program Grant Number JPMXD0220354483.

References

[1].H. Kuroda, K. Okazaki, K. Isoda, Toshiba Review, Vol. 70, No. 8, (2015), 49-53, (In Japanese).

[2].M. Gaillardin, S. Girardin, S. Girard, P. Paillet, J. L. Leray, V. Goihhon, et al., Investigations on the Vulnerability of Advanced CMOS Technologies to MGy Dose Environments, IEEE Trans. On Nuclear Science, Volume60, No.4, Augest, (2013), 2590-2597.

[3].N. Kuhns, L. Caley, A. Rahman, S. Ahmed, J. Di, H. A. Mantooth, et al., Complex High-Temperature CMOS Silicon Carbide Digital Circuit Designs, IEEE Trans. On Device and Materials Reliability, Vol.16, No.2, June, (2016), 105-111.

[4].H. Kappert, N. Kordas, S. Dreiner, U. Paschen, R. Kokozinski, High Temperature SOI CMOS Technology and Circuit Realization for Applications up to 300°C, IEEE International Symposium on Circuits and Systems (ISCAS), May, (2015), 1162-1165.

[5].R. Hedayati, L. Lanni, S. Rodriguez, B. G. Malm, A. Rusu, C.-M. Zetterling, A Monolithic, 500 ◦C Operational Amplifier in 4H-SiC Bipolar Technology, IEEE Electron Device Letters, Vol.35, July, (2014),

693-695.
[6].K. J. Chen, O. Häberlen, A. Lidow, C. l. Tsai, T. Ueda, Y. Uemoto, et al., GaN-on-Si Power Technology: Devices and Applications, IEEE Trans. on Electron Devices, Vol. 64, March, (2017), 779-794.
[7].M. Masunaga, S. Sato, R. Kuwan, N. Sugii, A. Shima, 4H-SiC CMOS Transimpedance Amplifier of Gamma-Irradiation Resistance Over 1 MGy, IEEE Trans. on Electron Devices, Vol. 67, January, (2020), 224-229.
[8].M. S. Lee, and H. C. Lee, Dummy Gate-Assisted n-MOSFET Layout for a Radiation-Tolerant Integrated Circuit, IEEE Trans. on Nuclear Science, Vol. 60, August, (2013), 3084-3090.
[9].V. V. Buniatyan, V. M. Aroutiounian, Wide gap semiconductor microwave devices, Journal of Physics D: Appliyed Physics, Vol.40, (2007), 6355-6385.
[10].T. Iwasaki, Y. Hoshino, K. Tsuzuki, H. Kato, T. Makino, M. Ogura, et al., High-Temperature Operation of Diamond Junction Field-Effect Transistors With Lateral p-n Junctions, IEEE Electron Device Letters, Vol.34, (2013), 1175-1177.
[11].B. A. Fox, M. L. Hartsell, D. M. Malta, H. A. Wynands, C.-T. Kao, L. S. Piano, et al., Diamond devices and electrical properties, Diamond Related Materials, No.4, (1995), 622-627.
[12].K. Ueda, M. Kasu, Y. Yamauchi, T. Makimoto, M. Schwitters, D.J. Twitchen, et al., Diamond FET Using High-Quality Polycrystalline Diamond With fT of 45 GHz and fmax of 120 GHz, IEEE Electron Device Letters, Vol.27, No.7, (2006), 570-572.
[13].K. Tsugawa, H. Noda, K. Hirose, H. Kawarada, Schottky barrier heights, carrier density, and negative electron affinity of hydrogen-terminated diamond, Physical. Review B, Vol.81, issue 4, (2010), 045303.
[14].H. Umezawa, S. Ohmagari, Y. Mokuno, J. H. kaneko, Characterization of X-Ray Radiation Hardness of Diamond Schottky Barrier Diode and Metal-Semiconductor Field-Effect Transistor, Proceedings of The 29th International Symposium on Power Semiconductor Devices & ICs, Sapporo, (2017), 379-382.
[15].J. H. Kaneko, etcl, Final Report of Inovative Research and Development program of MEXT, Research and Development Promotion Project for National Challenges Nuclear Energy Systems Research and Development Project Radiation Resistant and High Temperature for Innovation in Reactor Instrumentation Development of Operating Diamond Measurement System and Development of elemental technologies for diamond ICs, (2019), (In Japanese).
[16].N. H. Trung, N. Taoka, H. Yamada, T. Takahashi, T. Yamada, M. Shimizu, Experimental Demonstration of n- and p-channel GaN-MOSFETs toward Power IC Applications, ECS Journal of Solid State Science and Technology, Vol.9, No.1, (2020), 015001.
[17].M. Sometani, Y. Katsu, D. Nagai, H. Tsuji, T. Hosoi, T. Shimura, et al., Improved channel mobility of 4H-SiC n-MOSFETs by ultrahigh-temperature gate oxidation with low-oxygen partial-pressure cooling, Japanese journal of Aplied Physics, Vol.57, No.12, (2018), 120304.
[18].X. Zhang, T. Matsumoto, S. Yamasaki, C. E. Nebel, T. Inokuma, N Tokuda, Inversion-type p-channel diamond MOSFET issues, Journal of Materials Research, Vol.36, Issue23, (2021), 4688-4702.
[19].Z. Ren, G. Yuan, J. Zhang, L. Xu, J. Zhang, W. Chen, et al., Hydrogen-terminated polycrystalline diamond MOSFETs with Al_2O_3 passivation layers grown by atomic layer deposition at different temperatures, AIP Advances, Vol.8, Issue6, (2018), 065026.
[20].Z. Ren, D. Lv, J. Xu, J. Zhang, J. Zhang, K. Su, et al., High temperature (300 °C) ALD grown Al_2O_3 on hydrogen terminated diamond: Band offset and electrical properties of the MOSFETs, Applied Physics Letters, Vol.116, Issue 1, (2020), 013503.
[21].H. Kawarada, H. Tsuboi, T. Naruo, T. Yamada, D. Xu, A. Daicho, et al., C-H surface diamond field effect transistors for high temperature (400 °C) and high voltage (500 V) operation, Applied Physics Letters, Vol.105, (2014), 013510.
[22].T. Yamaguchi, H. Umezawa, S. Ohmagari, H. Koizumi, J. H. Kaneko, Radiation hardened H-diamond MOSFET (RADDFET) operating after 1 MGy irradiation, Applied Physics Letters Vol.118, Issue16, (2021), 162105.
[23].T. Masumura, H. Umezawa, T. Yamaguchi, Y. Deguchi, H. Kawashima, T. Makino, et al., Analysis of radiation resistance of Radiation hardened H-diamond MOSFET (RADDFET), New Diamond and Nano Carbons 2022, Poster Session 8P-12, 8 Jun, (2022).
[24].T. Masumura, Y. Deguchi, H. Umezawa, T. Makino, H. Kawashima, N. Hoshikawa, et al., Development of differential amplifier of Radiation hardened H-diamond MOSFET (RADDFET), New Diamond and Nano Carbons 2022, Session I-04 Electronic Devices 2, 7 Jun, (2022).

[25].S. Ohmagari, K.Srimongkon, H. Yamada, H. Umezawa, N. Tsubouchi, A. Chayahara, et al., Low resistivity p^+ diamond (100) films fabricated by hot-filament chemical vapor deposition, Diamond and Related Materials, Vol.58, (2015), 110-114.
[26].H Kawarada, Hydrogen-terminated diamond surfaces and interfaces,Surface Science Reports, Vol.26, Issue 7, (1996), 205-209.
[27].Y. Deguchi, H. Umezawa, T. Masumura, H. Kawashima, T. Makino, N. Hoshikawa, et al., Development of differential amplifier of Radiation hardened H-diamond MOSFET (RADDFET), The 36th Japan New Diamond Forum ,aural session 7-312, 19 November, (2022), (In Japanese).